Delft University of Technology

Effect of Cuff Compliance on Muscle Activation in a Passive Shoulder-Exotendon Suit

Degree: Master Mechanical Engineering
Program: ME-M-BMD-2019 - Master ME, track Biomechanical Design

Author:
Adrian Sahetapy
student ID:
4588827

Contributors:
A. Seth (supervisor)

Committee Members:
A. Seth
M. Prendergast
T. Van Wouwe

date:
24-12-2024

Effect of Cuff Compliance on Muscle Activation in a Passive Shoulder-Exotendon Suit

Adrian Sahetapy

December 2024

1 abstract

Exo devices allows users to decrease muscle effort by offloading it to the exo device. Compliance in the physical human-robot interface, originating from flexible cuffs and soft body tissue, can affect the forces transferred. The design of the cuff can alter the value of the pHEI compliance, but it is not yet known to what extent changes in pHEI compliance affect the muscle activation. Due to human variances and the difficulty of measuring objective performance metrics, it is difficult to experimentally pin point cause and effect. Therefore a novel model based method was used which combined experimentally obtained pHEI compliance data with musculoskeletal models to simulate the effect of pHEI compliance on muscle activation. A case study using this method was performed on a subject wearing a passive shoulder exotendon suit.
Results indicate a large effect of cuff design on stiffness, damping and cuff migration values.
Furthermore, optimising a rigid model and adding compliance afterwards resulted in an increase of total normalised muscle cost. Results from this compliant simulation let to results more closely representing EMG data from another study. Finally, optimising a compliant model results in a total normalised muscle cost equal to that of the rigid case, increased robustness of the exo to configuration errors and increased comfort. This indicates that compliance does not have a detrimental effect on optimised performance when taken into consideration during optimisation.

2 Introduction

The connection between exo and the wearer is inherently compliant due to the wearer's soft tissue and the flexible connection cuffs of the exo. This compliance in the exo's physical human-exo interface (pHEI) affects the performance of the

suit. Deformation and sliding of the pHEI leads to (non)elastic displacement of the cuff and deformation of the cuff and soft tissue, which can affect the forces transferred to the user [1–3]. These effects can affect the magnitude and timing of the forces transferred to the user [2, 4, 5], induce discomfort [1, 6–17] and in the worst case scenario cause tissue damage [18].

It has been shown that the design of the cuff can alter the way force is transferred through the pHEI. Cuff design parameters, such as the surface area of the cuff in contact with the skin [2, 6, 8, 11, 14], the cuff material [2, 11, 19–21] have the most prominent effect. Knowledge on how cuff design parameters affect performance measures are often taken from experimental data which are based on a large number of participants to exclude the impact of human variability on the outcome measures [6, 11, 12]. This makes it time consuming and expensive to analyse for any particular cuff. Furthermore, the structure of the muscles makes it difficult to measure EMG signals for the deeper lying muscles, such as trapezius, lattisimus dorsi and subscapularis, requiring invasive procedures such as indwelling EMG to be used [22].

Furthermore, these studies are limited to the scope of the pHEI itself and do not look into the exo-human system as a whole. System performance metrics such as muscle effort and perceived effort have been used before to describe musculoskeletal performance [23], but are lacking for compliant exo systems.

Efforts have been made to create computer models that can represent the compliance found in a pHEI of wearable robotic devices [3, 24–26]. Such models can give insight into the effect of pHEI compliance on objective outcome measures such as muscle activation and can at the same time decrease the reliance on time consuming experiments. Studies that simplified the exo-human system to be rigidly connected, however, resulted in large discrepancies between modeled performance and real performance [27, 28]. Movement of the cuff due to the pHEI compliance resulted in less force being transferred to the user. This lowered the effective assistance provided by the exo.

This study aims to present a model based approach that can adequately simulate the pHEI compliance in a passive shoulder exotendon suit and to analyse the effect pHEI compliance has on exosuit performance. To argue for the effectiveness of the method, 3 different cuff configurations will be tested whose parameters are experimentally determined. Afterwards the study of Joshi et al. [27], with its rigid model assumption, will be used as a comparison for the simulation results. Compliant elements are added a model of a passive shoulder exosuit that models the pHEI compliance. Its effect on the model will be discussed together with comparisons with experimental EMG data of the real exosuit. Finally the model will be optimised and analysed with compliance taken into consideration to see if compliance is detrimental to system performance.

3 Method

To study the effect of pHEI compliance on the muscle effort a OpenSim musculoskeletal shoulder model was be used. This model consists of a existing

shoulder and exosuit model with added bushing elements, which represent the compliant pHEI. These bushing elements displace from its rest position due to the force of the exosuit and apply forces to the body depending on the displacement and rate of displacement. As such the compliance in this model consists of 3 parameters: *rest position*, *stiffness* and *damping*.

Before the compliance can be inserted into a model of the suit, reference compliance parameters need to me measured. To do this we first measured the compliance of the cuffs of a existing exosuit. These parameters were then inserted into the OpenSim musculoskeletal model.

3.1 Passive Shoulder Exosuit

The Exosuit in question, shown in Fig.1, can be described as a passive shoulder exotendon suit. The suit provides assistance to the shoulder joint by storing and releasing energy in the spring system of the suit [27]. The suit stores energy when the arm is lowered and the spring is lengthened. During shoulder flexion the spring decreases in length and releases its energy to assist in the arm movement. The suit is connected to the body with a set of cuffs and straps on the pelvis, shoulder and arm and can be adjusted through the use of buckles and straps. The lack of rigid support structure and linkages commonly found in exoskeletons allow this exosuit to be optimally aligned to the wearers joint kinematics.

The experiment measured the cuff compliance of four cuffs: the thigh cuff and three possible arm cuff designs. The three arm cuff designs are shown in Fig.2 and can be described as such:
Design A,*Hand Cuff*, consists of a glove with nylon webbing that extends towards the upper arm. This allows the transfer of shear forces at the point of force application on the arm towards the glove worn on the hand [27].
Design B, *Tube Cuff*, consists of a modified off-the-shelf elbow brace. It's large surface area, compliant material makeup and pressure ensures that the cuff does not slip away while the interface forces are spread around a large surface area. Nylon webbing is used to create an attachment point for the exotendon. Modification of an already existing elbow brace has been done before [29].
Design C, *Elbow Cuff*, consists of a rectangular piece of fabric that is wrapped around the upper arm. It is made from compliant foam padding and reinforced with nylon webbing. This cuff emulates common tubular arm cuff designs [19, 30].

3.2 Equipment

Forces were measured by a Futek LSB series 50kg. load cell and output signal between -5V and 5V with a frequency of 20Hz. The data was processed through a National Instruments DAQ NI USB-6008 system. The Marker based motion capture was performed in the TU Delft Gait Lab. The output signal has a frequency of 100Hz. Sensor synchronisation was achieved by a 5V signal output from the motion capture rig to the DAQ, which then started the load

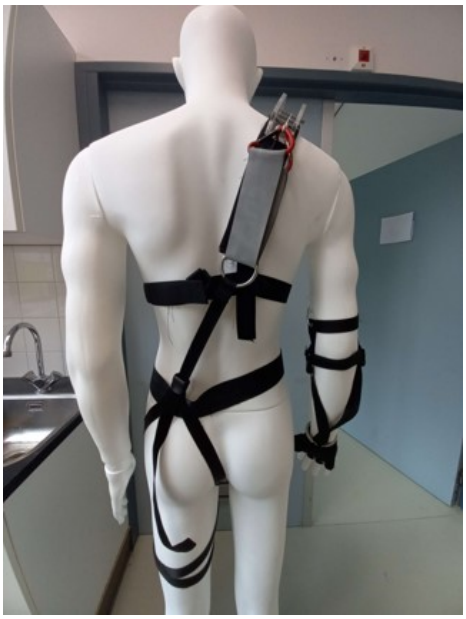

Figure 1: The analysed passive shouder exosuit. It consists of a waist cuff, shoulder cuff and arm cuff. Assistance is provided by a spring at the back of the user which extends and contracts depending on the position of the arm.

Figure 2: The three different arm cuff designs analyzed in the experiment:
(A):Hand cuff, where forces acting on the arm are transfered through webbing down towards the glove on the hand
(B):Elbow cuff, modification of commercially available elbow brace
(C):Tube cuff, tubular cuff designed to be easily donned by wrapping it around the arm

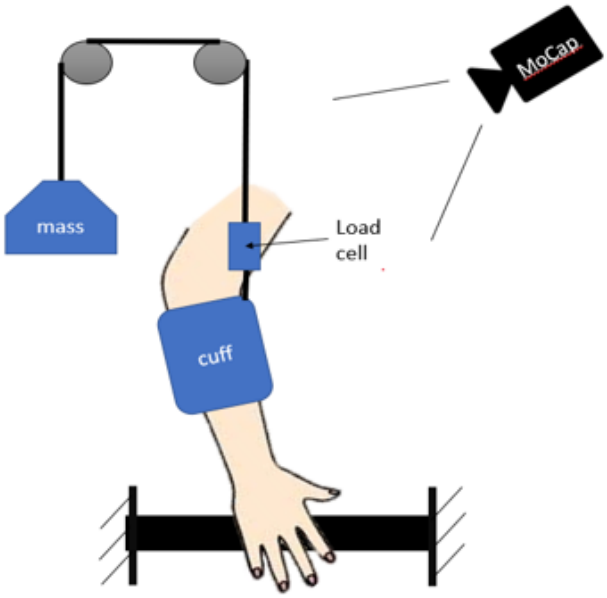

Figure 3: Schematic overview of the experiment setup. The subject wears the cuff and is asked to stand keep the body still. Force is applied to the cuff through a rope to which a weight is attached. A load cell above the rope attachment point measure the interaction force while the motion tracking cameras measure the movement of the body and the cuff.

cell measurement. Load cell data and motion lab data was synchronised by the measurement of a 5V start signal the labratory computer outputs when the motion measurement started.

3.3 Measuring cuff compliance

Fig.3 shows a schematic overview of the experiment setup. All measurements were measured from a single subject and were performed after getting approval by the Human Research Ethics Committee of the Delft University of Technology. At the start of the session the subject wore the to be examined cuff. The subject was asked to stand still next to the frame. A rope was led towards the cuff through a series of pulleys attached to the frame . The pulleys were set up such that the force vector of the rope on the cuff is similar to the force vector on the cuff during standard exosuit operation. When the measurement started, weights were attached to the other end of the rope which caused the rope to tug on the cuff. Since the subject stood still, the only displacement the cuff experienced was due to the force of the rope and the compliance of the pHRI. The load acting on the cuff was measured by a load cell measuring the tension between the cuff and the rope.

The displacement of the cuff was measured through the use of marker based motion capture data with markers attached to the bony landmarks of the body according to the *Qualisys Sports Marker Set*. To detect movement of the cuff, markers were place on the cuff at the attachment point to the rope.

The experiment itself consisted of two measurements which were repeated three times. The first measurement was the static load measurement. The weights and the accompanying forces in the static test were increased stepwise. After a weight was attached the cuff displaced under the newly applied load. Forces and displacements were recorded when the human-exosuit system reached steady state.

The second measurement was a dynamic load measurement. The weights and the accompanying forces in the dynamic tests were applied in a sinusoidal pattern by inserting a spring between the end of the rope and the weight. When the weight was perturbed, the spring caused a sinusoidal force to be applied to the cuff. Force and displacement was measured continuously for this test.

These two tests were repeated 3 times with a 1 minute break between them. The cuff itself was only donned once. It was not taken off between tests. The whole routine was repeated for each tested cuff resulting in 24 measurements (4 cuffs, 2 measurements, repeated 3 times).

3.4 Data processing

Two sets of data were extracted from the experiment: load cell data and marker data. Both measurements started using the same input signal and were thus already synchronized.

The computation of cuff displacement data was done by comparing the displacement of the cuff marker data against the displacement of the anchoring body marker data. In case of the waist cuff, the anchoring body was the torso with markers placed on the shoulders, sternum, back of the lower waist. In case of the three different arm cuffs, the anchoring body was the upper arm with markers placed on the shoulder and on the elbow.

Extracting the stiffness and damping value from the force and displacement data was done by assuming the system to be equivalent to an ideal spring-damper system:

$$F_{loadcell} = k_{cuff} x_{relative} + c_{cuff} \dot{x}_{relative} \tag{1}$$

To extract the stiffness of the cuff the steady stepwise force data of the first test was used. The dynamic component of the measurement was ignored and only the points representing steady force were used in the measurement where $\dot{x}_{relative} = 0$. Since $\dot{x}_{relative} = 0$, eq.1 simplifies to the formula for an ideal spring shown in eq.2. A linear fit was made to the data where the slope of the fit represents the stiffness of the cuff.

$$F_{loadcell} = k_{cuff} x_{relative} \tag{2}$$

To get the damping value of the cuff the data from the dynamic measurement were used together with the newly calculated stiffness value of the cuff. Assuming the ideal mass-damper system the force measured in the load cell can be split into the elastic component, F_k, and the damper component, F_c:

$$F_{loadcell} = F_k + F_c \tag{3}$$

$$F_{loadcell} - F_k = F_{loadcell} - k_{cuff} x_{relative} = F_c = c_{cuff} \dot{x}_{relative} \tag{4}$$

From this a linear fit was made to the load and velocity data where the velocity is calculated by differentiating the position data. The slope of the fit represented the damping value of the cuff.

The cuff migration was the final component to be measured. This equaled the displacement of the cuff at the end of the static measurement. Since the initial position of the cuff was taken as x=0, the final cuff position after the measurement was finishing and all the load is released from the cuff was the actual position the cuff should be attached to. The difference between the final position, $x_{relative,end}$, and the initial position, $x_{relative,start}$, was taken as the cuff migration value, $l_{migration}$:

$$l_{migration} = x_{relative,end} - x_{relative,start} \tag{5}$$

3.5 Musculoskeletal model

The thoracoscapular model is used as the base model for the simulation and can be seen in Fig.4. The model consists of 11 degrees of freedom and 33 muscles that accurately simulate shoulder movement [23, 31]. This model can be posed in certain ways by providing it with motion data consisting of position and velocity values for each degree of freedom (DoF) of the model. The motion data for this study is taken from the shoulder motion data set from a shoulder study done by Belli et al. [32].

The exosuit is attached on the existing shoulder model. It consists of a pathspring element with an independent spring constant, damping value and rest length. The pathspring is led from the attachment point on the pelvis over the shoulder to the attachement point on the humerus. The distance between the two attachment points changes as the body moves about. This change of length of the pathspring results in a force being applied proportional to the elongation compared to its rest length and the rate of its elongation.

3.6 modelling pHEI compliance

Compliance was added to the pHEI according to the method presented by Zhou et al. [3] where visco-elastic bushing elements were used as connecting points between the exo and the skeleton body. This method was adapted to be used for the model of a compliant shoulder exosuit. To simulate the pHEI compliance

additional body elements, representing the cuffs, were added to the model and placed where the pathspring originally attached to the body.

For the purposes of this study the pHEI of this exo was divided into 3 cuffs. Arm, shoulder and pelvis cuffs. Of these cuffs only the pelvis and arm cuffs were modeled to have compliance. This was done because the force acting on these cuffs act in the same axis as the underlying bone and parallel to the skin surface, where the compliance is largest [33, 34]. The shoulder cuff experiences forces normal to the skin surface. This in combination with the existence of only a thin tissue layer above the clavicle and scapula led to the assumption that the shoulder cuff experiences insignificant compliance effects compared to the pelvis and arm cuffs. It was further assumed that the mass of the exosuit, 600gr [27], is evenly divided across the 3 cuffs.

The bodies of these cuffs were simplified and modeled as hollow cylinders [35]. The mass, dimensions and inertia can be found in TABLE.1.

	mass [kg]	radius [m]	thickness [mm]	Ixx [kg][m]^2($x10^{-2}$)	Iyy [kg][m]^2($x10^{-2}$)	Izz [kg][m]^2($x10^{-2}$)
Pelvis	0.2	0.15	2	0.06122	0.06122	0.07444
Arm cuff	0.2	0.06	2	0.2321	0.2321	0.4560
Shoulder	0.2	-	-	-	-	-

Table 1: mass, dimension and inertia parameters for the 3 cuffs used in the model

The pathspring connects to these cuff body elements. The cuff body elements of the arm and pelvis in turn attach to the skeleton body through the use of bushing elements. These bushing elements act as a 3 degree of freedom spring element with stiffness and damping values. This allows them to freely move about 3 axis of translation relative to the skeleton body it is attached to. It applies force to the skeleton body proportional to its position relative to its rest position and proportional to its velocity relative to the anchoring body part. Due to the design of the exo the exotendon lies flat against the skin surface as it wraps around the shoulder and connects to the arm and pelvis. This results in the line of force being parallel to the skin surface and being largely independent of shoulder angle. Since the direction of the force vector acting on these bushing elements does not change much relative to the cuff, for the scope of this study, it is assumed that the stiffness and damping can be described through as isotropic.

3.7 Estimating the bushing force

To estimate the effect of pHEI on the exo performance the bushing force needws to be calculated. This bushing force depends on the state of the cuff which consists of position and velocity data. This cuff moves under influence of the pathspring force and the bushing force. These forces of the exosuit are in turn a function of the state $\boldsymbol{q}$ and joint velocity $\dot{\boldsymbol{q}}$ on each timestep, k.
For the rigid model condition the tension in the exotendon is expressed as:

$$\boldsymbol{F}_{spring,k} = k_{spring} x(\boldsymbol{q_k}) \tag{6}$$

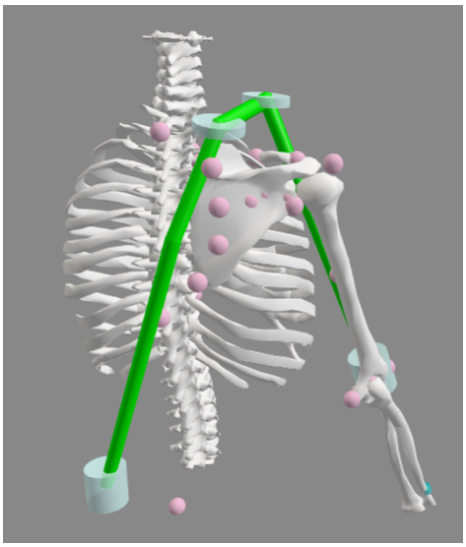

Figure 4: The musculoskeletal OpenSim model. the green line represents the spring and can extend and contract as the right arm lowers and rises. Compliant interface points are represented as cylinders on the arm and waist and can be switched between rigid and compliant configuration to analyse the effect of compliance on the simulation.

For the visco-elastic model conditions the force exerted by any given bushing element, b, is expressed as:

$$\boldsymbol{F}_{b,k} = k_{b,k}\boldsymbol{q}_{b,k} + c_{b,k}\dot{\boldsymbol{q}}_{b,k} \tag{7}$$

The bushing position $\boldsymbol{q}_b$ was estimated by solving for equilibrium for a given state of the skeleton. The skeleton was locked into a pose given by the positional data in $\boldsymbol{q}_k$. The velocities were set to zero, $\dot{\boldsymbol{q}}_k = \boldsymbol{0}$. The cuffs were allowed to move freely. Using forward simulation the cuffs could move under the influence of the force of the pathspring $\boldsymbol{F}_{spring,k}$ and bushing forces $\boldsymbol{F}_{b,k}$. This continues until the forces in any given cuff are such that:

$$\sum \boldsymbol{F}_k = \boldsymbol{F}_{spring,k} + \boldsymbol{F}_{b,k} = \boldsymbol{0} \tag{8}$$

All the simulated bushing states were collected in $\boldsymbol{q}_b$. $\dot{\boldsymbol{q}}_b$ was derived by differentiation:

$$\dot{\boldsymbol{q}}_{bush,k+1} = \frac{\boldsymbol{q}_{bush,k+1} - \boldsymbol{q}_{bush,k}}{\Delta t} \tag{9}$$

The bushing state was then added to the original motion data to get the complete motion data set with states $\boldsymbol{q}_{new} \in \mathbb{R}^{(N_q+N_r)}$, which was used in the simulation.

3.8 Calculating muscle activation

To get the muscle activation from the model the 'Rapid Muscle Redundancy' (RMR) solver was used. It can estimate the required muscle activation for a given OpenSim model and movement data [32]. This is achieved by minimizing the sum of the weighted squares of muscle activations and actuator controls, while following anatomically justified constraints, with particular emphasis on the glenohumeral constraint:

$$J(\boldsymbol{a_k}, \boldsymbol{c_k}) = \sum_{i=0}^{N_m} w_i a_{i,k}^2 + \sum_{j=0}^{N_q} v_i c_{j,k}^2 \tag{10}$$

Where N_m is the number of muscles of the model and N_q the number of actuated joints. $a_{i,k}$ and $v_{j,k}$ represent the muscle activation and actuator control of muscle i and actuator j respectively at timestep k of the motiondata.

The activation and control values need to solve the following statement:

$$\ddot{\boldsymbol{q}}_j^d = \ddot{\boldsymbol{q}}(a, v_j) \tag{11}$$

where $\ddot{\boldsymbol{q}}_j^d$ is the desired acceleration of skeleton joint j, taken from the movement data, and $\ddot{\boldsymbol{q}}(a, v_j)$ is the simulated acceleration affected by muscle activation and actuator control.

3.9 Model conditions

To analyse the effect of pHEI compliance, compliance was added to the model and each model configuration was analysed. Two conditions could be turned on and off on the model which had the following effects:

Cuff Migration: Cuffs can migrate away from the original attachment site after cycles of loading and unloading [36]. The shear forces in the pHEI have to be counteracted by friction. If at the original attachment site the friction is not enough, it will displace across the skin surface in the direction of the force until a new equilibrium is reached. When the cuff is unloaded the cuff has permanently migrated from its original position. The values used here were the cuff migration values extracted from the experiment as seen in TABLE.2.

Visco-elasticity: To analyse the effect of the visco-elastic component of pHEI compliance, the visco-elastic bushing elements can be turned on and off. The values inserted here were the stiffness and damping values extracted from the experiment as seen TABLE.2.

3.10 Analysing the effect of compliance on muscle effort

First a comparison was made against the optimal rigid model. To do this the rigid model was be used to optimise the exo. This was done by using a gridsearch strategy on the 1 configurable parameter of the exosuit, the exotendon rest length L_0. The rest length that minimised the cost of eq.10 was deemed to be

the optimal exo configuration. The optimal rest length was then used on the compliant model configurations.
Next, the data was compared against experimental EMG data from the shoulder exosuit study of Joshi. et al [27]. Finally, the exo rest length optimisation was repeated on the compliant model configurations.

4 Results

4.1 Effect of cuff design on compliance values

The output of the cuff measuring experiments for the hand cuff can be seen in Fig.5 with the displacement vs time data in the upper graph and force vs time data in the bottom half. The complete data set consists of 12 static measurements and 12 dynamic measurements taken from a single subject and can be found in Appendix.A.

As can be seen in the figure the displacement of the cuff rises at the same time as the load applied to the cuff. This confirms the idea that cuffs displace when loads are applied. Plotting the displacement against the force of the static measurements results the the curve seen in Fig.6. Points of stepwise force increase are circled on the curve. A red line shows a linear fit of the data with the slop representing the stiffness extracted.

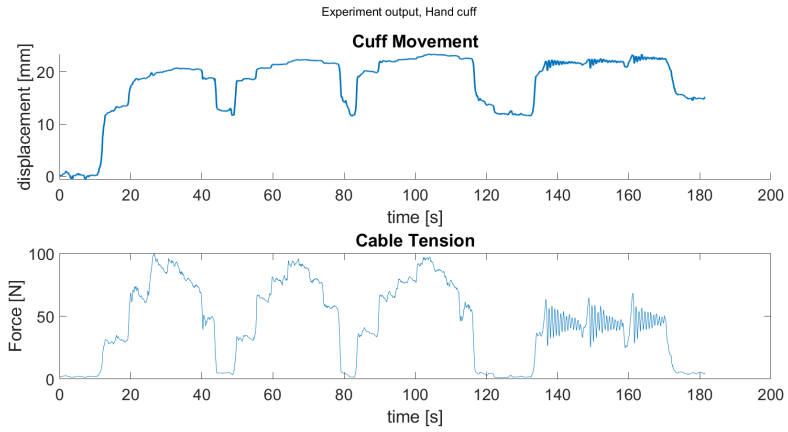

Figure 5: Output hand cuff measurement for load cell (above) and motion capture rig (below) vs time. The start and end of each measurement is indicated by the dashed vertical lines.

The fit of the damping value on the dynamic load data is shown in Fig.7, with its angle representing the damping value of the cuff. The stiffness and damping fits of the other measurements can be seen in Appendix.B

The resulting cuff stiffness, damping and migration data can be seen in TABLE.2. This resulted in stiffness values of [2140-8520]N, damping values of

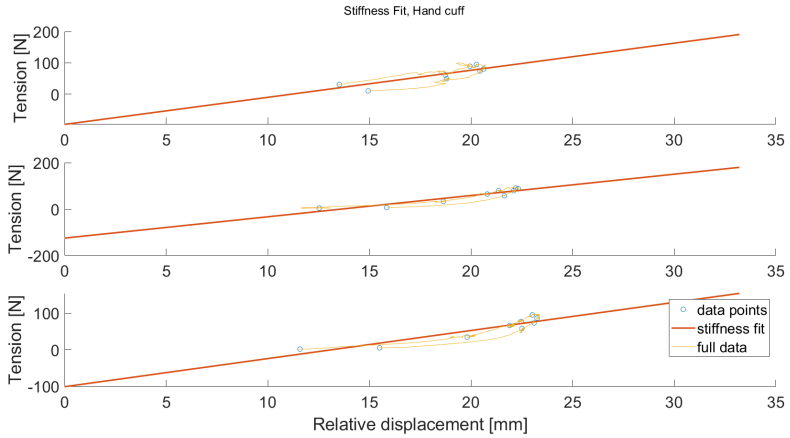

Figure 6: Stiffness fitted according to eq.2 to data of one static load measurement of the hand cuff

	Stiffness $[N][m]^{-1}$	damping $[N][s][m]^{-1}$	Cuff migration $[cm]$
Waist	2140	124	1.2
Hand cuff	8520	210	1.2
Tube cuff	5510	38	0.9
Elbow cuff	2530	139	2.2

Table 2: Calculated compliance values for the four tested cuffs

[38-210]Nm/s and migration values of [0.9-2.2]cm.

4.2 Effect of assuming rigid model on compliant model

Optimising the exo's rest length to minimise the total muscle activation results in the graph seen in fig.8 results in a optimal rest length for the exotendon of L_0=0.74 meter.

Analysing the effect of assuming a rigid model on a compliant system results in data seen in TABLE.3. It can be seen that between shifting the cuff and adding visco-elastic elements to the cuff, the cuff shift leads to a larger difference between total normalised muscle cost compared to the fully rigid model

	No assitance	Rigid	Rigid + shift	Visco-elastic	Visco-elastic + shift
Design A	1	0.787	0.829	0.798	0.858
Design B	1	0.787	0.829	0.803	0.854
Desing C	1	0.787	0.869	0.818	0.877

Table 3: Total muscle activation normalised against a no assistance muscle activation.

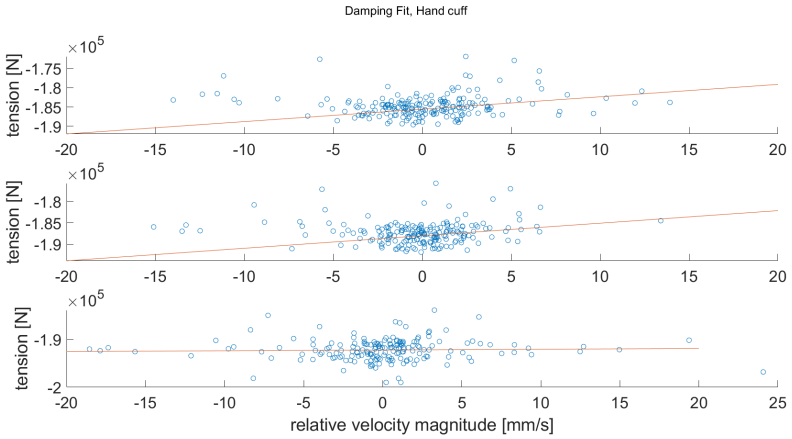

Figure 7: Damping fitted according to eq. to data of one dynamic load measurement of the hand cuff

condition.

A detailed look into specific muscle activations is shown in Fig.9. It can be seen that in general the no-assistance curve and the rigid curve are the bounds of minimal and maximum activations. The other model conditions lie somewhere in between those two curves. Specifically for the medial serratus using the any exo seems increase the amount of muscle activation required. Data for the other cuffs can be found in Appendix.C

4.3 Comparison between EMG and rigid and compliant simulation

Analysing the reduction in muscle effort between EMG and simulated data shown in Fig.10 shows that the compliant simulation corresponds better with experimental EMG data. EMG data of the anterior and posterior deltoid, trapezius superior and serratus shows better correspondence with the compliant model condition compared to the rigid model condition. EMG data for the medial deltoid, however, does not correspond well to either rigid or compliant simulation.

4.4 Effect of compliance on optimal exosuit configuration

Fig.11 shows the total muscle cost normalized against the condition's respective 'no assistance' case. It shows a decrease in normalized total muscle cost as the rest length decreases, which increases again as the rest length continues to shorten. Curves for the other cuffs can be found in Appendix.D

Looking at the value of the rest length at the minimum of the normalized total muscle activation in TABLE4 shows that rest length decreases with in-

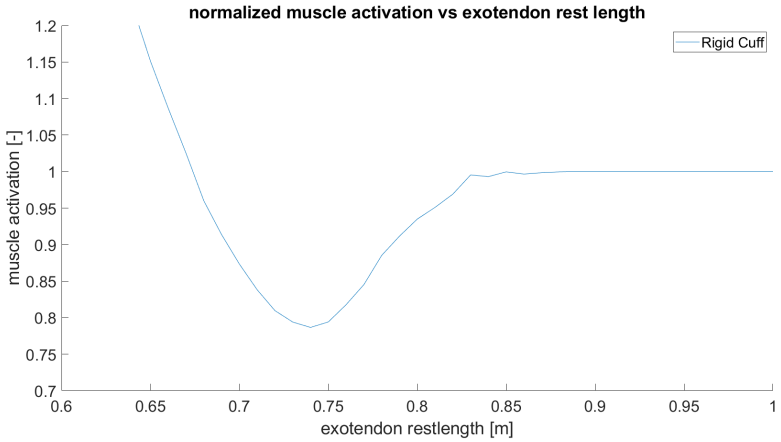

Figure 8: The total normalised muscle activation as a function of exo rest length. A clear minima can be seen.

creasing compliance. At the same time the normalised total muscle cost stays the same.

A third observation is that the width of the valley changes with increasing compliance. This value represents the permissable rest length error and can be seen in the fourth column of TABLE4. From this data it can be seen that the model conditions with the visco-elastic elements show a larger permissable rest length error compared to the model conditions with no visco-elastic elements.

5 Discussion

5.1 Effect of cuff design on pHEI compliance

TABLE2 shows extracted cuff compliance values for the 4 different cuffs. It shows that different cuff designs have large impact on stiffness values.
Effect of cuff design on cuff migration values seem small. However compared to the exosuit spring extension seen in Fig.8, the difference in exotendon rest length between the optimal configuration and being too large to provide assistance can be as small as 10cm. A cuff migration value up to 2.2 cm results in a decrease of maximum assistive force by 22%. Thus small migration values can have large effects on effective assistance.
More specific statements on the effect of cuff design on compliance can not be made currently as the designs differ too much from each other to compare a single design parameters. Another study could analyse this further.

Looking at the data of Fig.7 shows that the values on the y-axis are negative. A closer look at Fig.5 could provide an explanation. The displacement during the static load and the dynamic load test are similar in magnitude, but the load is a lot smaller during the dynamic test. Subtracting the elastic force component

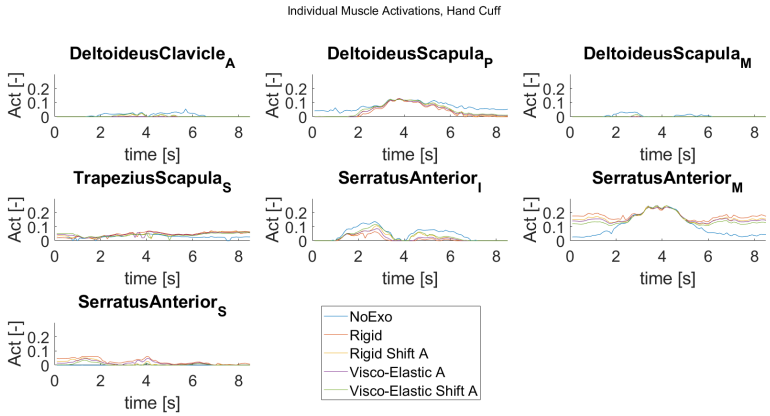

Figure 9: Detailed muscle activation of primary muscle involved in shoulder flexion. Multiple conditions are shows using parameters of the hand cuff (Design A) using exotendon rest length of 0.74m

from the dynamic load measurement results in the damper force component becoming negative. This means that a significant part of the pHEI dynamics is not being represented by the current spring damper model. Possible explanations could be the existence of a significant effect of the angle of the interaction force vector relative to the cuff, indicating that the compliance is anisotropic. This could impact the modelling results in cases where the interaction force vector changes significantly during the motion.

5.2 Effect of assuming rigid model on compliant model

When you do not optimise with compliant cuffs in mind and you assume a rigidly connected exosuit, it can be seen in TABLE3 that as compliance increases, the total normalised muscle cost increases and thus the effective assistance decreases.

Furthermore, comparing the difference between shifted and rigid conditions, and visco-elastic and rigid conditions shows that the shifted cuff results in a larger difference in total normalised muscle cost. This indicates that cuff shifting has a larger effect on exo performance. Design A and B have similar muscle costs in this regards, with only design C differing in the same model condition. This corresponds to a cuff migration value of [0.9-1.2]cm and 2.2cm respectively. This indicates that a 1cm difference could result in a 5% point increase in total normalised muscle cost, demonstrating the exo's sensitivity to exotendon rest length.

Looking into the visco-elastic model it can be seen that between design A,B and C there is only a 2% point difference, even though the measured stiffness of the cuff ranges between 8520N and 2530N and the damping between 210Ns/m and 38Ns/m. This indicates a low sensitivity to stiffness and damping values.

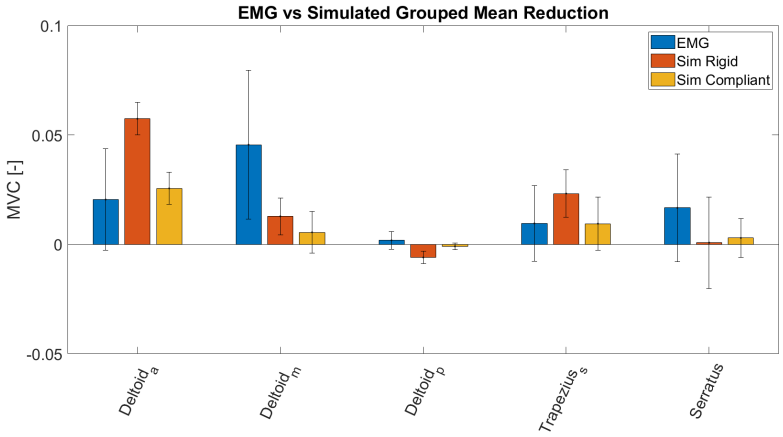

Figure 10: Comparison of muscle activation reduction between assisted and non-assisted condition of the EMG, and simulated rigid and compliant results, using the rigid model conditions's optimal exosuit configuration.

However, just these values existing in the model will lead to a change in total normalised muscle cost relative to the full rigid model, indicating that even small amounts of compliance will lead to an effect on performance.

A look into the data seen in Fig.9 showcases how using the exosuit could help alleviate muscle effort from the deltoids. It can further be seen that the rigid model, which reduces the total normalised muscle cost the most, also leads to the largest reduction in individual muscle activation in the deltoid muscles and in the inferior serratus. However, the rigid model also leads to the largest increase in muscle cost in the medial serratus. This indicates how the exosuit transfers load from one muscle group to the other, while as a whole lowering the total effort expended by the body.

5.3 Comparison between EMG and rigid and compliant simulation

The comparison of the reduction in muscle activation between the EMG data and simulated rigid and compliant data, seen in Fig.10, shows that the compliant simulation corresponds better with EMG data than the rigid simulation. Addition of compliance lower the mean EMG reduction to levles comparable of the EMG data, while rigid simulation results in values multiple times higher than the EMG data. This shows that the model using compliant cuffs is a better representation of the actual shoulder exosuit than the model using rigid cuffs.

Still existing differences between simulation and experimental EMG could be explained by:
the use a non scaled model while the experiment was done on multiple subjects, lack of experimental motion data in combination with imperfect reproduction

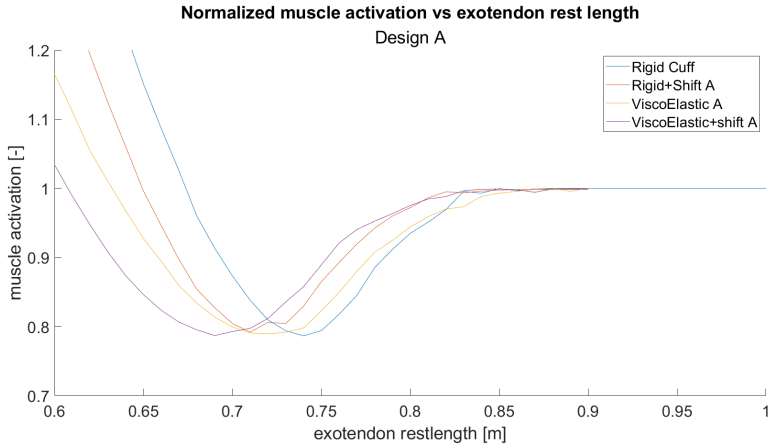

Figure 11: The effect of increasing compliance using the hand cuff parameters on the total muscle activation normalized against a 'no assistance' condition. Each conditions shows a clear minimum muscle cost at a different rest length value

of flexion motion during the experiment.
A future experiment with proper simulated scaling and proper motion tracking could result in a even better correspondence between experimental EMG and simulated muscle effort.

5.4 Effect of compliance on optimal exosuit configuration

As can be seen in Fig.11 and TABLE4 as compliance increases with addition of cuff migration and visco-elastic connection points the optimal rest length decreases. The total normalized muscle cost, however, does not decrease, indicating that in the optimized case the cuff compliance does not affect exosuit performance. This goes against the idea that adding compliance to a system decreases the performance of a system. An explanation could be that relative change between the no assistance case and the optimized case is the same for all conditions. As long as the exotendon can be stretched enough to provide the force required for minimising the muscle cost the compliance of the exosuit does not matter. The dynamic forces due to the cuff movement along the arm and the pelvis is not large enough to significantly effect the resulting muscle activation.

An aspect that does change is the width of the valley which increases as the compliance becomes larger, exact values can be seen in the fourth column of TABLE4. This value represents the allowed configuration error away from the optimal rest length where the user would still get 90% of the optimal assistance of the suit. Due to the additional compliance of the pHEI the lumped stiffness of the human exosuit system decreases. It thus takes a bigger stretch of the exo-

Model conditions	Optimal exotendon rest length [m]	Normalized muscle cost [-]	Permissable rest length error [cm]
Rigid	0.74	0.79	3.9
Rigid Shift [H]	0.71	0.79	4.1
Rigid Shift [T]	0.72	0.79	3.9
Rigid Shift [E]	0.71	0.78	3.7
Visco-elastic [H]	0.72	0.79	5.2
Visco-elastic [T]	0.72	0.79	5.4
Visco-elastic [E]	0.70	0.79	6.0
Visco-elastic + Shift [H]	0.70	0.79	5.3
Visco-elastic + Shift [T]	0.70	0.79	5.4
Visco-elastic + Shift [E]	0.68	0.79	5.8

Table 4: Effect of 4 model conditions using cuff parameters of the 3 arm cuffs on the outcome measures.
Model conditions: Rigid, Shift (cuff migration), Visco-elastic (cuff compliance), visco-elast + shift. Arm cuffs: [H] hand cuff, [T] tube cuff, [E] elbow cuff.
outcome measures: optimal exotendon rest length is the rest length of the adjustable exotendon to gain minimal muscle effort, normalized muscle cost is the normalized total muscle cost compared to the respective no assistance case, permissable rest length error is the configuration error that still provides 90% of the total muscle effort reduction.

tendon for the suit to provide the same force when the suit is attached with more compliant connections. A small deviation in the rest length leads to a smaller change in force output when more compliant connections are used. This also causes the force output to change more gradually as the exotendon extends and contracts, possibly resulting in a more comfortable wear. Adding compliance could thus decrease the suit sensitivity to the rest length and increase the allowable configuration error of, resulting in a suit that could be more comfortable and reduce the effect of human variance on exosuit performance.

6 Conclusion

We examined the effect of cuff compliance on the muscle effort for a passive shoulder exosuit. Experimental measurements of multiple cuffs of multiple cuffs showed that cuff stiffness, cuff damping and cuff migration are affected by cuff design and can lead to significant exosuit assistance reduction when not taken into consideration. Next, through simulations it is shown that when rigid model assumptions are made, adding compliance to the model causes a reduction in effective assistance by increasing the total normalised muscle cost. Comparing this data to experimental EMG values showcased how compliant models can more closely resemble the real data compared to rigid models. However, optimising with compliance in mind results in assistance levels equal to those resulting from the rigid model assumption. Furthermore, compliance increase the permissible configuration error thus maken the exo more robust to config-

uration errors and increase comfort on the user. This indicates that physical compliance with the human-robot interface (pHEI) does not have a detrimental effect on optimum exo performance but has a positive effect as it increase robustness and comfort.

The results of the experiment performed in this study showed that the current model lacks information to accurately model cuff compliance. Future studies could be conducted to measure the three dimensional compliance parameters of the cuffs allowing the model to be used in cases where the interaction force vector significantly changes during movement.

In summary, this study presents a promising way to analyse the effect of cuff compliance on the performance of a passive shoulder exosuit. The framework presented in this study could easily be extended to cuffs on other parts of the body such as the shanks or forearms, aiding in future studies on the effect of compliance on exosuit performance.

References

[1] M. B. Yandell, D. M. Ziemnicki, K. A. McDonald, and K. E. Zelik, "Characterizing the comfort limits of forces applied to the shoulders, thigh and shank to inform exosuit design," *PLOS ONE*, vol. 15, p. e0228536, Feb. 2020.

[2] B. Quinlivan, A. Asbeck, D. Wagner, T. Ranzani, S. Russo, and C. Walsh, "Force Transfer Characterization of a Soft Exosuit for Gait Assistance," in *Volume 5A: 39th Mechanisms and Robotics Conference*, (Boston, Massachusetts, USA), p. V05AT08A049, American Society of Mechanical Engineers, Aug. 2015.

[3] X. Zhou and L. Zheng, "Model-Based Comparison of Passive and Active Assistance Designs in an Occupational Upper Limb Exoskeleton for Overhead Lifting," *IISE transactions on occupational ergonomics and human factors*, vol. 9, no. 3-4, pp. 167–185, 2021.

[4] S. Lee and H. In, "Evaluating the effectiveness of an active strap for wearable robot: A Mechanical and Physiological Study," 2023.

[5] M. B. Yandell, B. T. Quinlivan, D. Popov, C. Walsh, and K. E. Zelik, "Physical interface dynamics alter how robotic exosuits augment human movement: implications for optimizing wearable assistive devices," *Journal of NeuroEngineering and Rehabilitation*, vol. 14, p. 40, Dec. 2017.

[6] T. Graven-Nielsen, H. B. Vaegter, S. Finocchietti, G. Handberg, and L. Arendt-Nielsen, "Assessment of musculoskeletal pain sensitivity and temporal summation by cuff pressure algometry: a reliability study," *Pain*, vol. 156, pp. 2193–2202, Nov. 2015.

[7] T. Kermavnar, K. J. O'Sullivan, V. Casey, A. de Eyto, and L. W. O'Sullivan, "Circumferential tissue compression at the lower limb during walking, and its effect on discomfort, pain and tissue oxygenation: Application to soft exoskeleton design," *Applied Ergonomics*, vol. 86, p. 103093, July 2020.

[8] T. Kermavnar, K. J. O'Sullivan, A. de Eyto, and L. W. O'Sullivan, "Discomfort/Pain and Tissue Oxygenation at the Lower Limb During Circumferential Compression: Application to Soft Exoskeleton Design," *Human Factors*, vol. 62, pp. 475–488, May 2020.

[9] T. Kermavnar, K. J. OSullivan, A. de Eyto, and L. W. OSullivan, "The effect of simulated circumferential soft exoskeleton compression at the knee on discomfort and pain," *Ergonomics*, vol. 63, pp. 618–628, May 2020. Publisher: Taylor & Francis _eprint: https://doi.org/10.1080/00140139.2020.1743373.

[10] T. Kermavnar, K. J. OSullivan, A. de Eyto, and L. W. OSullivan, "Relationship Between Interface Pressures and Pneumatic Cuff Inflation Pressure at Different Assessment Sites of the Lower Limb to Aid Soft Exoskeleton Design," *Human Factors*, vol. 63, pp. 1061–1075, Sept. 2021. Publisher: SAGE Publications Inc.

[11] . Kozinc, J. Babi, and N. arabon, "Human pressure tolerance and effects of different padding materials with implications for development of exoskeletons and similar devices," *Applied Ergonomics*, vol. 93, p. 103379, May 2021.

[12] J. Bessler-Etten, L. Schaake, J. H. Buurke, and G. B. Prange-Lasonder, "Investigating change of discomfort during repetitive force exertion though an exoskeleton cuff," *Applied Ergonomics*, vol. 115, p. 104055, Feb. 2024.

[13] Y. Wang, J. Qiu, H. Cheng, and X. Zheng, "Analysis of HumanExoskeleton System Interaction for Ergonomic Design," *Human Factors*, p. 0018720820913789, Mar. 2020. Publisher: SAGE Publications Inc.

[14] N. Zhao, X. Wang, and M. Tian, "Study on the Influence of Cuff Width and Air Pressure on Human Discomfort of Simulated Circumferential Soft Lower Limb Exoskeleton Compression," in *2021 IEEE 8th International Conference on Industrial Engineering and Applications (ICIEA)*, pp. 68–72, Apr. 2021.

[15] S. V. Sarkisian, M. K. Ishmael, and T. Lenzi, "Self-Aligning Mechanism Improves Comfort and Performance With a Powered Knee Exoskeleton," *IEEE Transactions on Neural Systems and Rehabilitation Engineering*, vol. 29, pp. 629–640, 2021. Conference Name: IEEE Transactions on Neural Systems and Rehabilitation Engineering.

[16] R. Andrade, J. Figueiredo, P. Fonseca, J. Vilas-Boas, M. Silva, and C. Santos, "Human-Robot Joint Misalignment, Physical Interaction, and Gait Kinematic Assessment in Ankle-Foot Orthoses," *Sensors*, vol. 24, no. 1, 2024.

[17] R. Diteesawat, S. Hoh, E. Pulvirenti, N. Rahman, L. Morris, A. Turton, M. Cramp, and J. Rossiter, "A Soft Fabric-based Shrink-to-fit Pneumatic Sleeve for Comfortable Limb Assistance," vol. 2022-October, pp. 9766–9773, 2022.

[18] X. Mao, Y. Yamada, Y. Akiyama, S. Okamoto, and K. Yoshida, "Safety verification method for preventing friction blisters during utilization of physical assistant robots," *Advanced Robotics*, vol. 31, pp. 680–694, July 2017. Publisher: Taylor & Francis _eprint: https://doi.org/10.1080/01691864.2017.1318716.

[19] M. Xiloyannis, D. Chiaradia, A. Frisoli, and L. Masia, "Characterisation of Pressure Distribution at the Interface of a Soft Exosuit: Towards a More Comfortable Wear," in *Wearable Robotics: Challenges and Trends* (M. C. Carrozza, S. Micera, and J. L. Pons, eds.), (Cham), pp. 35–38, Springer International Publishing, 2019.

[20] X. Wan, Y. Liu, Y. Akiyama, and Y. Yamada, "Monitoring Contact Behavior During Assisted Walking With a Lower Limb Exoskeleton," *IEEE Transactions on Neural Systems and Rehabilitation Engineering*, vol. 28, pp. 869–877, Apr. 2020. Conference Name: IEEE Transactions on Neural Systems and Rehabilitation Engineering.

[21] L. Levesque, S. Pardoel, Z. Lovrenovic, and M. Doumit, "Experimental comfort assessment of an active exoskeleton interface," in *2017 IEEE International Symposium on Robotics and Intelligent Sensors (IRIS)*, (Ottawa, ON), pp. 38–43, IEEE, Oct. 2017.

[22] S. I. Backus, D. P. Tomlinson, B. Vanadurongwan, M. W. Lenhoff, F. A. Cordasco, E. L. Chehab, R. S. Adler, R. F. Henn III, and H. J. Hillstrom, "A spectral analysis of rotator cuff musculature electromyographic activity: surface and indwelling," *HSS Journal®*, vol. 7, no. 1, pp. 21–28, 2011.

[23] A. Seth, M. Dong, R. Matias, and S. Delp, "Muscle contributions to upper-extremity movement and work from a musculoskeletal model of the human shoulder," *Frontiers in neurorobotics*, vol. 13, p. 90, 2019.

[24] S. Yousaf, G. Mukherjee, R. King, and A. Deshpande, "Experimental and Simulation-Based Estimation of Interface Power during Physical Human-Robot Interaction in Hand Exoskeletons," *IEEE Robotics and Automation Letters*, vol. 9, no. 3, pp. 2575–2581, 2024.

[25] S. N. Yousaf, P. Esmatloo, K. Ghonasgi, and A. D. Deshpande, "A Method for the Analysis of Physical Human-Robot Interaction," in *2021*

IEEE/ASME International Conference on Advanced Intelligent Mechatronics (AIM), pp. 1249–1254, July 2021. ISSN: 2159-6255.

[26] H. Sabzali, M. Fouji, M. Javanbakht, I. Kardan, and A. Akbarzadeh, "Effect of Slippage on Knee Exoskeleton Comfort," pp. 183–188, 2023.

[27] S. Joshi, I. Beck, A. Seth, and C. D. Santina, "Minimalistic Soft Exosuit for Assisting the Shoulder via Biomechanics-Aware Optimization," in *2022 IEEE-RAS 21st International Conference on Humanoid Robots (Humanoids)*, pp. 667–673, Nov. 2022. ISSN: 2164-0580.

[28] M. Cherry, S. Kota, A. Young, and D. Ferris, "Running With an Elastic Lower Limb Exoskeleton," *Journal of Applied Biomechanics*, vol. 32, June 2016.

[29] F. Missiroli, N. Lotti, E. Tricomi, C. Bokranz, R. Alicea, M. Xiloyannis, J. Krzywinski, S. Crea, N. Vitiello, and L. Masia, "Rigid, soft, passive, and active: A hybrid occupational exoskeleton for bimanual multijoint assistance," *IEEE Robotics and Automation Letters*, vol. 7, no. 2, pp. 2557–2564, 2022.

[30] K. Langlois, D. Rodriguez-Cianca, B. Serrien, J. De Winter, T. Verstraten, C. Rodriguez-Guerrero, B. Vanderborght, and D. Lefeber, "Investigating the Effects of Strapping Pressure on Human-Robot Interface Dynamics Using a Soft Robotic Cuff," *IEEE Transactions on Medical Robotics and Bionics*, vol. 3, pp. 146–155, Feb. 2021. Conference Name: IEEE Transactions on Medical Robotics and Bionics.

[31] A. Seth, R. Matias, A. P. Veloso, and S. L. Delp, "A biomechanical model of the scapulothoracic joint to accurately capture scapular kinematics during shoulder movements," *PloS one*, vol. 11, no. 1, p. e0141028, 2016.

[32] I. Belli, S. Joshi, J. M. Prendergast, I. Beck, C. Della Santina, L. Peternel, and A. Seth, "Does enforcing glenohumeral joint stability matter? a new rapid muscle redundancy solver highlights the importance of non-superficial shoulder muscles," *PLOS ONE*, vol. 18, pp. 1–19, 11 2023.

[33] Z. Sun, B. D. Gepner, S.-H. Lee, J. Rigby, P. S. Cottler, J. J. Hallman, and J. R. Kerrigan, "Multidirectional mechanical properties and constitutive modeling of human adipose tissue under dynamic loading," *Acta Biomaterialia*, vol. 129, pp. 188–198, 2021.

[34] M. Takaza, K. M. Moerman, J. Gindre, G. Lyons, and C. K. Simms, "The anisotropic mechanical behaviour of passive skeletal muscle tissue subjected to large tensile strain," *Journal of the mechanical behavior of biomedical materials*, vol. 17, pp. 209–220, 2013.

[35] R. Hibbeler, K. Yap, and S. Fan, *Mechanics for Engineers: Dynamics*. Always Learning, Pearson, 2013.

[36] M. Xu, Z. Zhou, J. Shao, L. Ruan, and Q. Wang, "Reducing migration of knee exoskeletons with dynamic waist strap," *IEEE Transactions on Medical Robotics and Bionics*, vol. 4, no. 3, pp. 764–774, 2022.

A Experiment Output

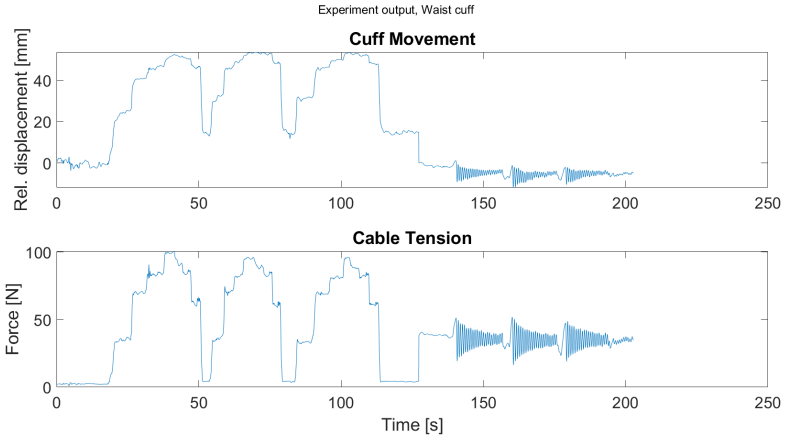

Figure 12: Experimental output consisting of static load and dynamic load measurement for the waist cuff. Up: motion data, Down: load cell data

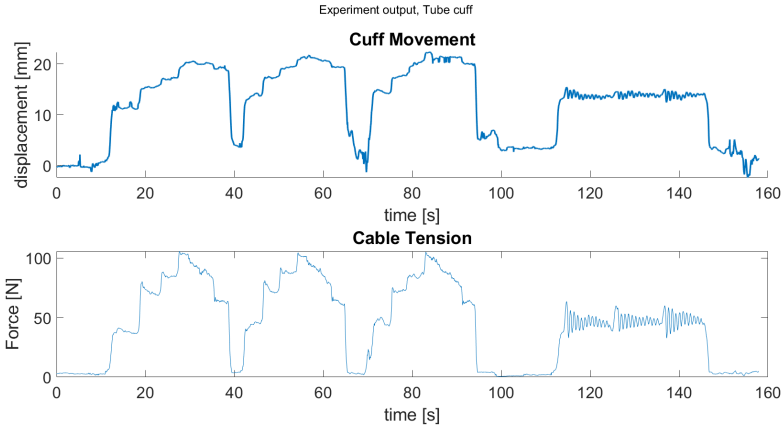

Figure 13: Experimental output consisting of static load and dynamic load measurement for the Tube cuff. Up: motion data, Down: load cell data

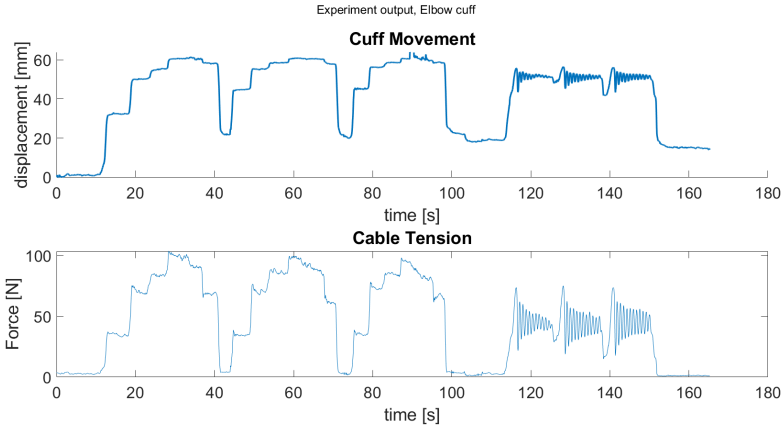

Figure 14: Experimental output consisting of static load and dynamic load measurement for the Elbow cuff. Up: motion data, Down: load cell data

B Stiffness and Damping fits

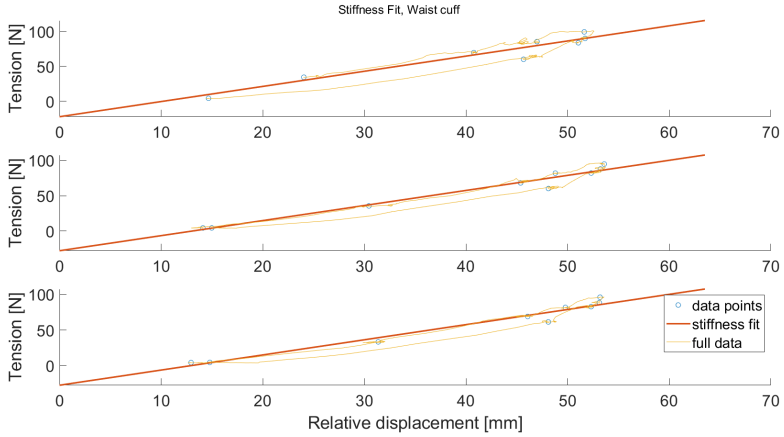

Figure 15: Stiffness fit on the 3 static load measurements for the waist cuff

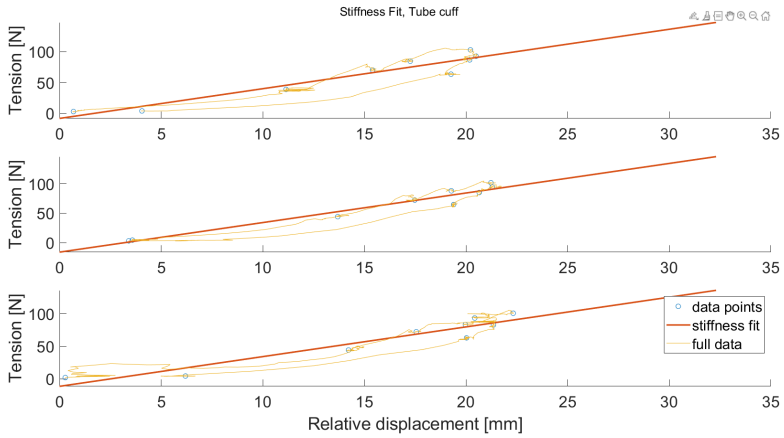

Figure 16: Stiffness fit on the 3 static load measurements for the tube cuff

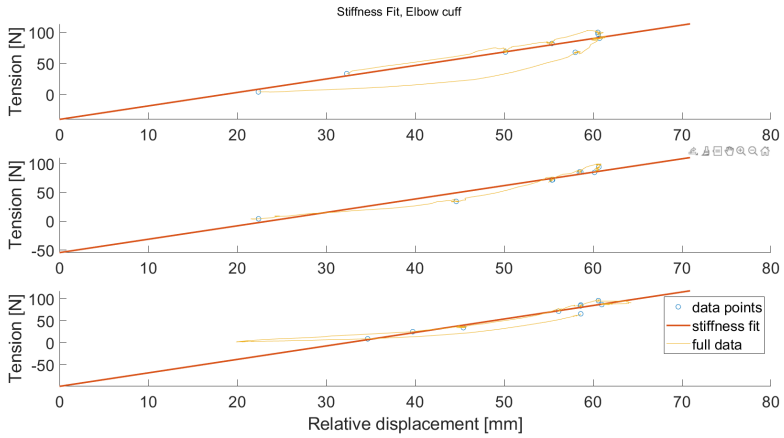

Figure 17: Stiffness fit on the 3 static load measurements for the elbow cuff

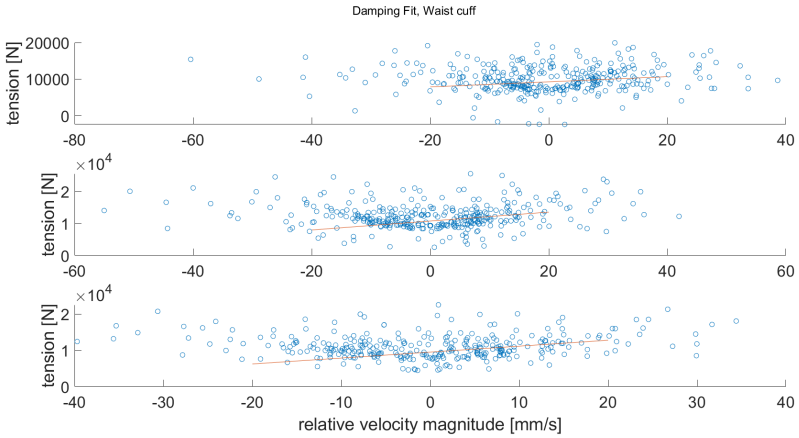

Figure 18: Damping fit on the 3 static load measurements for the waist cuff

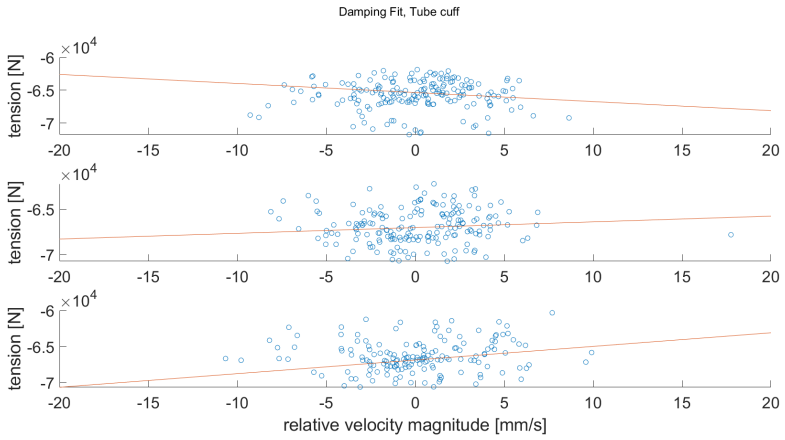

Figure 19: Damping fit on the 3 static load measurements for the tube cuff

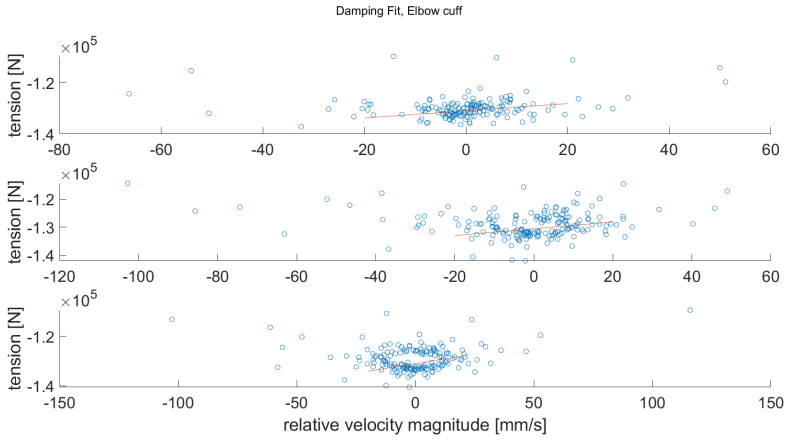

Figure 20: Damping fit on the 3 static load measurements for the elbow cuff

C Individual muscle activations

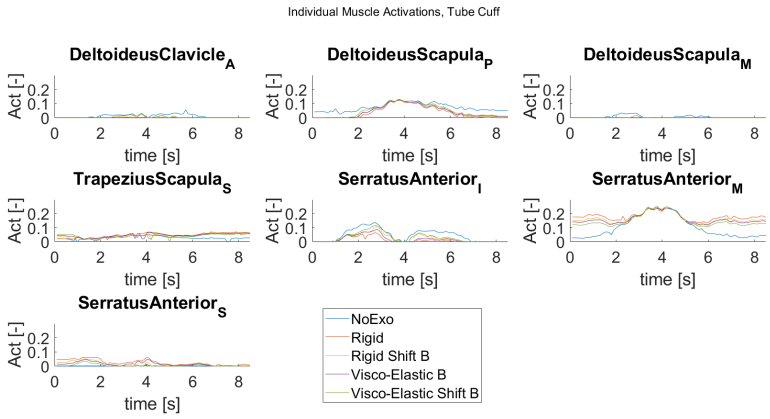

Figure 21: Comparison of muscle activation using optimal rigid exo configuration. Use of parameters from the tube cuff (Design B)

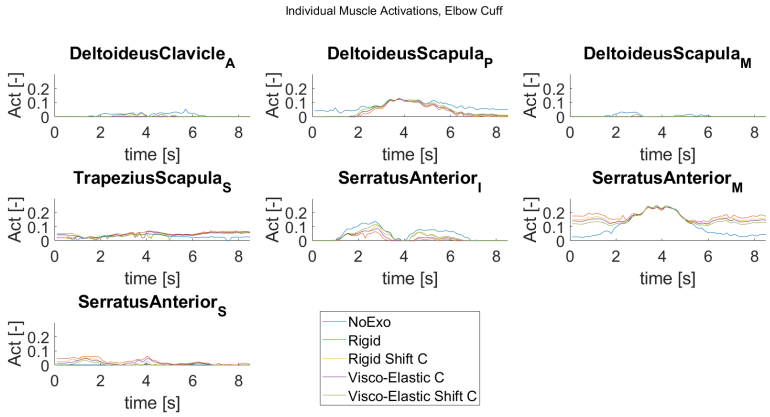

Figure 22: Comparison of muscle activation using optimal rigid exo configuration. Use of parameters from the elbow cuff (Design C)

D Optimising Exo Restlength with Compliance

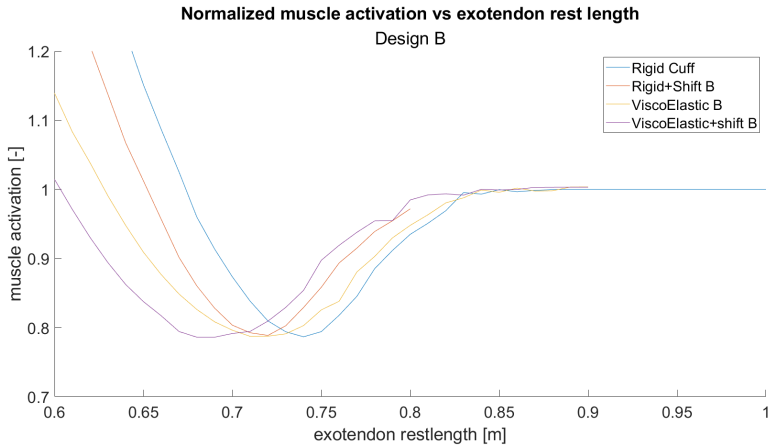

Figure 23: Total muscle cost of different model conditions using parameters from the tube cuff (Design B) normalised against the total muscle cost of a exo configuration that does not provide assistance

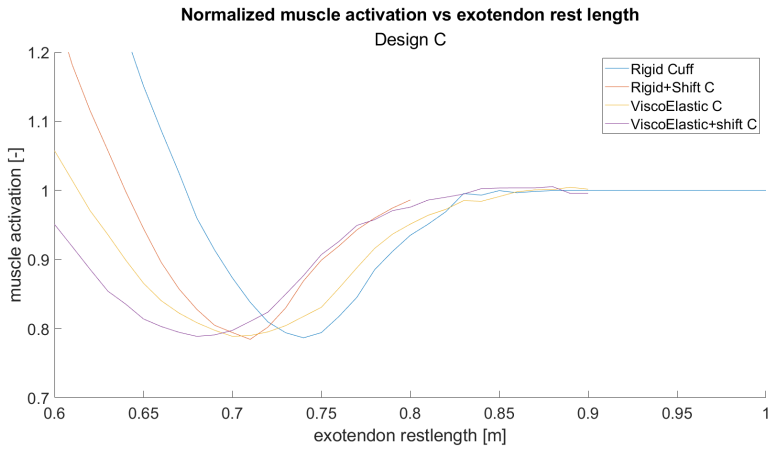

Figure 24: Total muscle cost of different model conditions using parameters from the elbow cuff (Design C) normalised against the total muscle cost of a exo configuration that does not provide assistance